Construction and Building Materials 25 (2011) 4126–4131

Contents lists available at ScienceDirect

Construction and Building Materials

journal homepage: www.elsevier.com/locate/conbuildmat

Acoustic emission characterization of the fracture process in fibre reinforced concrete

D.G. Aggelis *, D.V. Soulioti, N. Sapouridis, N.M. Barkoula, A.S. Paipetis, T.E. Matikas

Dept. Materials Science and Engineering, University of Ioannina, Ioannina 45110, Greece

ARTICLE INFO

Article history:
Received 10 April 2010
Received in revised form 5 April 2011
Accepted 14 April 2011
Available online 7 May 2011

Keywords:
Acoustic emission
Bending
Concrete
Fracture
Pull-out
Steel fibres

ABSTRACT

The present study occupies with the characterization of the fracture process of steel fibre reinforced concrete. Different acoustic emission indices are correlated with the accumulation of damage and the type of source. The amplitude distribution of the acquired signals is very sensitive to micro-cracking, while individual mechanisms like matrix cracking and fibre pull-out can be distinguished by the average frequency of the corresponding signals which exhibits a severe decrease at the moment of main. As a result, acoustic emission can be used as a warning against the failure of this material while the broadband transducers can be used to characterize the different damage mechanisms.

1. Introduction

Steel fibre reinforced concrete (SFRC) is being increasingly employed in structural applications. Fibres improve the material in terms of ductility and strength. The fibre action increases the possibility that the crack growth will be delayed [1]. Consequently, the total absorbed fracture energy is increased mitigating catastrophic phenomena. Fracture in such a material starts with matrix cracking followed by the failure of different interfaces; i.e. between cement paste and sand, aggregates and fibres. Final failure includes aggregate crushing and fibre rupture [2]. The post peak behaviour is governed by the fibre pull-out events. Generally, the fracture of SFRC can be divided in three stages. The "stable micro-cracking", where the micro-cracks' grow until they reach a saturation threshold, the rapid expansion of the cracks followed by macroscopic fracture and the post peak behaviour where pull-out events dominate.

In order to clarify the above mechanisms, acoustic emission (AE) monitoring has been applied during four-point bending tests on SFRC specimens. The AE technique has been employed in numerous applications for damage characterization of materials and processes [3–7], including concrete and large structures [8–13]. Suitable sensors are placed on the surface in order to record the transient waves (hits) generated by the crack propagation incidents inside the material. Subsequently, the characterization and quantification of the damage level is performed via the use of appropriate AE descriptors. Further study of the transient waveforms provides in depth insight of the fracture process. The source of the AE activity is closely connected to the mode of fracture [14]. The ultimate goal of this approach is the possible implementation in a remote monitoring procedure of large structures. Therefore, AE parameters which are sensitive to the dynamic nature of fracture are sought for. Recent studies on SFRC have shown that specific AE indices like the average frequency, AF, or the rise angle of the AE waveforms are well correlated with the accumulation of damage [15]. Additionally, features based on the amplitude distribution of the AE signals act as a pre-cursor of final fracture. These features are briefly described later in the text.

2. Experimental details

The specimens used in this study were 100 × 100 × 400 mm in size. The water to cement ratio by mass was 0.5 and the maximum aggregate size was 10 mm. The fibre content was 1% by volume, while the shape of the fibres was wavy with length of 25 mm and diameter of 0.75 mm. After mixing and forming, the fibres are assumed to be randomly oriented and distributed. The specimens were tested in four-point bending. The bottom and top spans were 300 mm and 100 mm respectively, as seen in Fig. 1a. The monotonic displacement rate was 0.08 mm/min and the maximum mid span deflection was 2 mm according to ASTM C1609/C 1609 M-05. Details on the mechanical testing can be found in [16]. It is noted that all specimens failed with a central crack that extended from the bottom tensile side to the top, as opposed to the diagonal cracks that are exhibited in concrete reinforced with metal bars. Two AE broadband sensors (Pico, PAC) were attached to the bottom tensile side of the specimen (Fig. 1b). Roller bearing grease was used for acoustic coupling while the sensors were secured by the use of electric mounting tape during the experiment. The signals were recorded in a two-channel monitoring board PCI-2, PAC with a sampling rate of 5 MHz.

* Corresponding author. Tel.: +30 26510 08006; fax: +30 26510 08054.
E-mail address: daggelis@cc.uoi.gr (D.G. Aggelis).

0950-0618/$ - see front matter © 2011 Elsevier Ltd. All rights reserved.
doi:10.1016/j.conbuildmat.2011.04.049

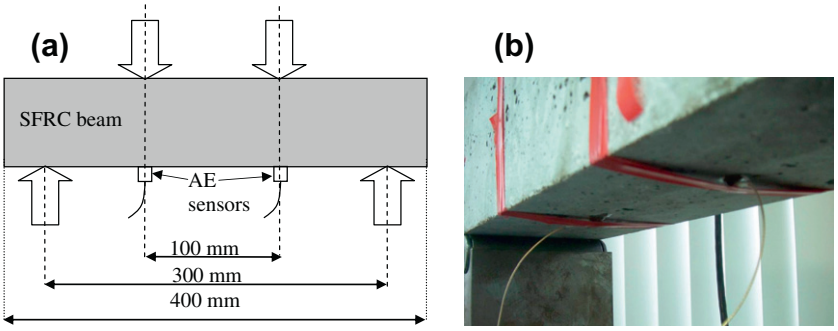

Fig. 1. (a) Schematic representation of four-point bending of concrete with AE monitoring. (b) A close up of the AE sensors during experiment.

3. AE parameters

It is understandable that the rate of incoming AE activity is of primary importance, since high rate of AE recording is connected to high rate of crack propagation incidences, while no AE activity implies no serious crack propagation. Thus, the total number of AE hits recorded relatively to the measurement time is the first and crucial parameter of the test.

However, many more parameters are valuable. According to the individual failure mechanisms that can be active inside a material, the emitted signals may differ considerably. For example in concrete, failure includes matrix cracking, as well as detachment between aggregates and cement paste. If the material contains fibres, then fibre pull-out also contributes to the final failure. The distinct fracture mechanisms emit AE signals with different characteristics. Therefore, many parameters of the recorded waves are calculated in order to facilitate the analysis and enhance the characterization of the distinct failure mechanisms [17]. A typical AE waveform is seen in Fig. 2, along with its main characteristics.

One crucial characteristic of AE testing is the level of the "threshold" which is set by the user. It should be set at a value high enough to avoid the acquisition of weak ambient noise (environment, electrical) but on the same time low enough to allow recording of the actual cracking signals. Some of the basic parameters of the AE signals are the arrival time (onset), which is the moment of the first threshold crossing, the "Amplitude, A", which is the maximum voltage (either in Volts or dB) exhibited by the highest peak of the waveform, the "Duration" which is the time span in μs, between the first and the last threshold crossing. The total number of threshold crossings is called "Counts", while the time between the onset and the peak of the highest cycle is called "Rise Time, RT" in μs. The ratio of Amplitude to Rise Time is called Rise Angle or Grade in literature [5,18]. Recently the inverse is utilised (RA = Rise Time/Amplitude, μs/V) as suggested by the relevant technical committee [17]. The number of Counts divided by the duration is called "average frequency, AF".

In general, the amplitude corresponds to the scale of fracture, since the energy emitted from the source depends on the crack opening displacement; small displacement emits waves of low energy, while large crack propagation incidences generate higher amounts of energy. Characteristics like RA and AF have been correlated to the cracking type (tensile or shear) as will be discussed in more detail later.

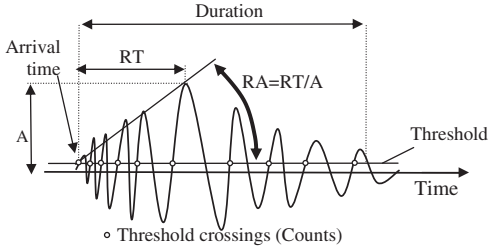

Fig. 2. Typical AE waveform.

3.1. Ib-value

Different fracture modes generate different types of acoustic emission signals with varying frequency ranges and amplitudes. Micro-cracks generate a large number of small amplitude acoustic emissions. Macro-cracks generate not so many events as micro-cracks do; however, the macro-cracks are of higher amplitude. When macro-cracking events occur, a high amount of the elastic energy is released and consequently mostly small amplitude events develop. The occurrence of primary events alters the stress field in the neighbourhood of the source region. Therefore, it is reasonable to affect also the relative distribution of small and large events. The "I*b*-value" represents the ratio of weak to strong events [19]. As mentioned above, micro-cracks generate a large number of weak acoustic emissions. Therefore, micro-cracking leads to a relatively high I*b*-value, which is the absolute value of the slope of the cumulative distribution of the amplitudes of the recent 50 hits (see Fig. 3). Macro-cracking, instead, leads to relatively low *b*-values since it creates relatively more of the strong events. With increasing stress levels, the fracture process moves from micro- to macro-cracking and the I*b*-value decreases. Thus, an I*b*-value decrease can be interpreted as a successive stress accumulation due to a propagating rupture front. For the original analysis of I*b*-value, the interested reader is directed to the original work of Shiotani et al. [20].

The formula for the I*b*-value calculation is defined as:

$$\mathrm{I}b = \frac{\log_{10} N(\mu - \alpha_1 \cdot \sigma) - \log_{10} N(\mu + \alpha_2 \cdot \sigma)}{(\alpha_1 + \alpha_2)\sigma} \quad (1)$$

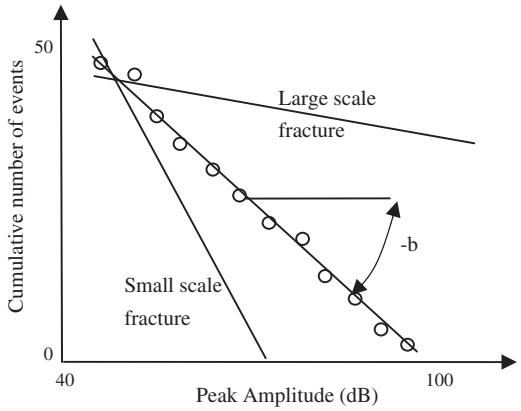

Fig. 3. Acoustic emission peak amplitude cumulative distribution.

where σ is the standard deviation of the magnitude distribution of one group of recent hits (in our case 50), μ is the mean value of the magnitude distribution of the same group of events, and α_1 and α_2 are constants that define which part of the population will be taken into account. Usually α_1 and α_2 are given the values of 0 and 1 respectively and the population, N, of recent hits employed in the calculation is 50 or 100. It is understood that the I*b*-value is a transient feature, updated with each new hit recorded during the fracture process.

A typical Load and AE cumulative hits vs. Time curve is shown in Fig. 4a. The rate of AE hits is progressively increasing as the load reaches the maximum value. At the moment of fracture, which is evident by the drop of the load from approximately 12 kN to 7 kN, the AE hit rate exhibits a maximum as seen by the almost vertical hit line. At that moment more than 200 hits are recorded. After the load drop, the AE rate decreases but the activity does not stop. Concerning the mechanical behaviour, in most cases after the first macro-crack develops, load drops by several kN. Only in one specimen (Fig. 4e) the maximum is reached after the first major crack formation. This behaviour is not unusual for SFRC [16]. In Fig. 4b–f the I*b*-value time history is depicted for all individual specimens. For each specific case, a strong drop of the I*b* curve is exhibited much earlier than the load drop and is marked by an arrow. In Fig. 4b the I*b*-value history of the same specimen presented in Fig. 4a is shown. The I*b*-value exhibits a strong decrease at the time of 368–370 s (see arrow), while the load is at approximately 62% of the maximum. At that point the number of hits did not show any particular change as can be seen in Fig. 4a. The decrease of I*b*-value occurs for all five specimens with wavy fibres much earlier than the maximum load. In one case, the I*b* drop is noted as early as 38% of the maximum load (Fig. 4f). Overall, the drop of I*b*-value occurs much earlier or approximately at 80% of the maximum load for any of the examined cases, giving thus a warning well before the macroscopic fracture. This drop is attributed to cracking incidents which do not strongly influence the global hit rate but they have an effect on the amplitude distribution of the hits. The I*b*-value is a parameter which consistently acts as a warning much earlier than macroscopic failure. Therefore, its use in case of remote monitoring of large structures should be stressed out. Apart from the early drop of I*b*-value, the minimum value of each I*b* curve was exhibited at the moment of fracture, (values of approximately 0.03). In literature the value of 0.05 is generally considered the threshold below which severe damage is indicated [18–21]. Although in laboratory conditions identification of the

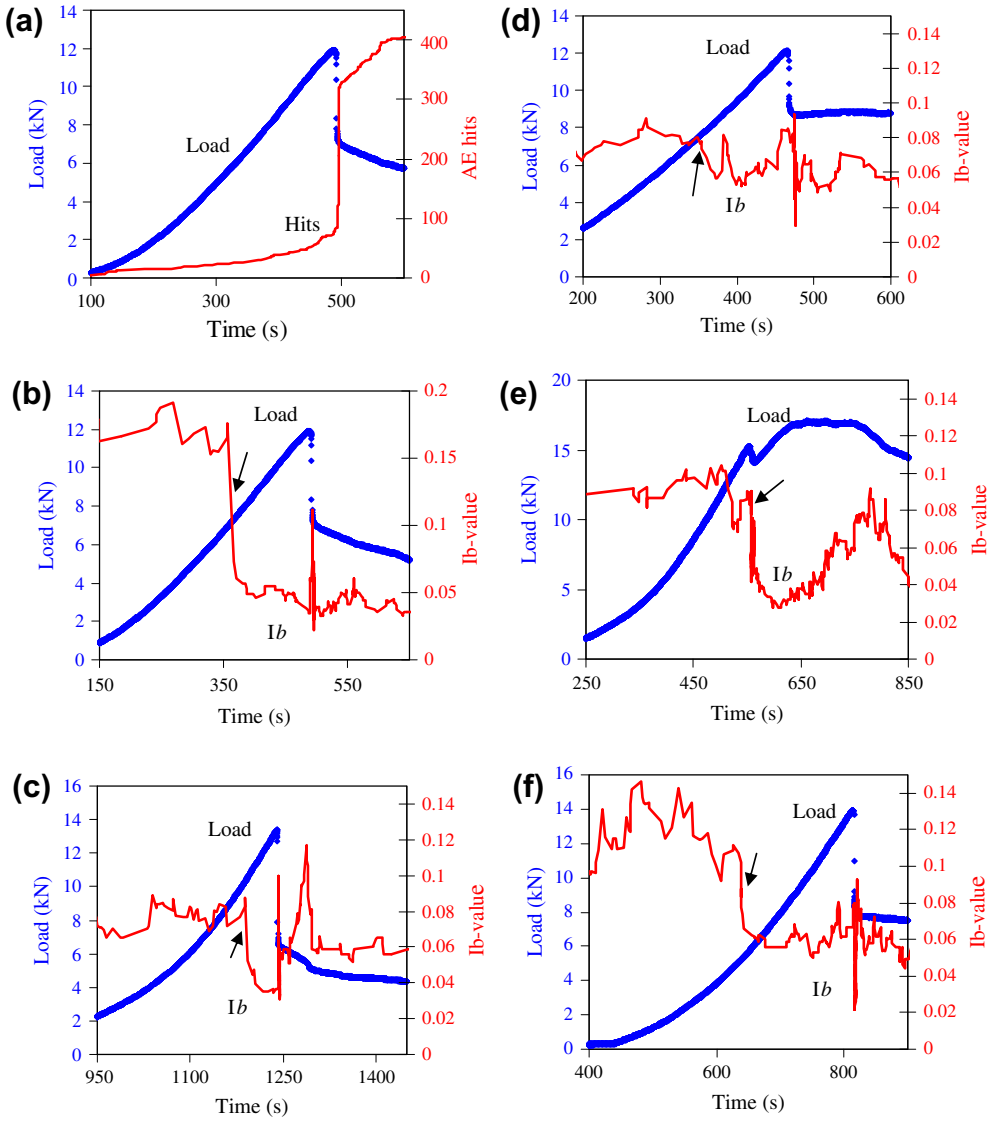

Fig. 4. Load and AE hits cumulative history, (b–f) load and I*b*-value history for all specimens.

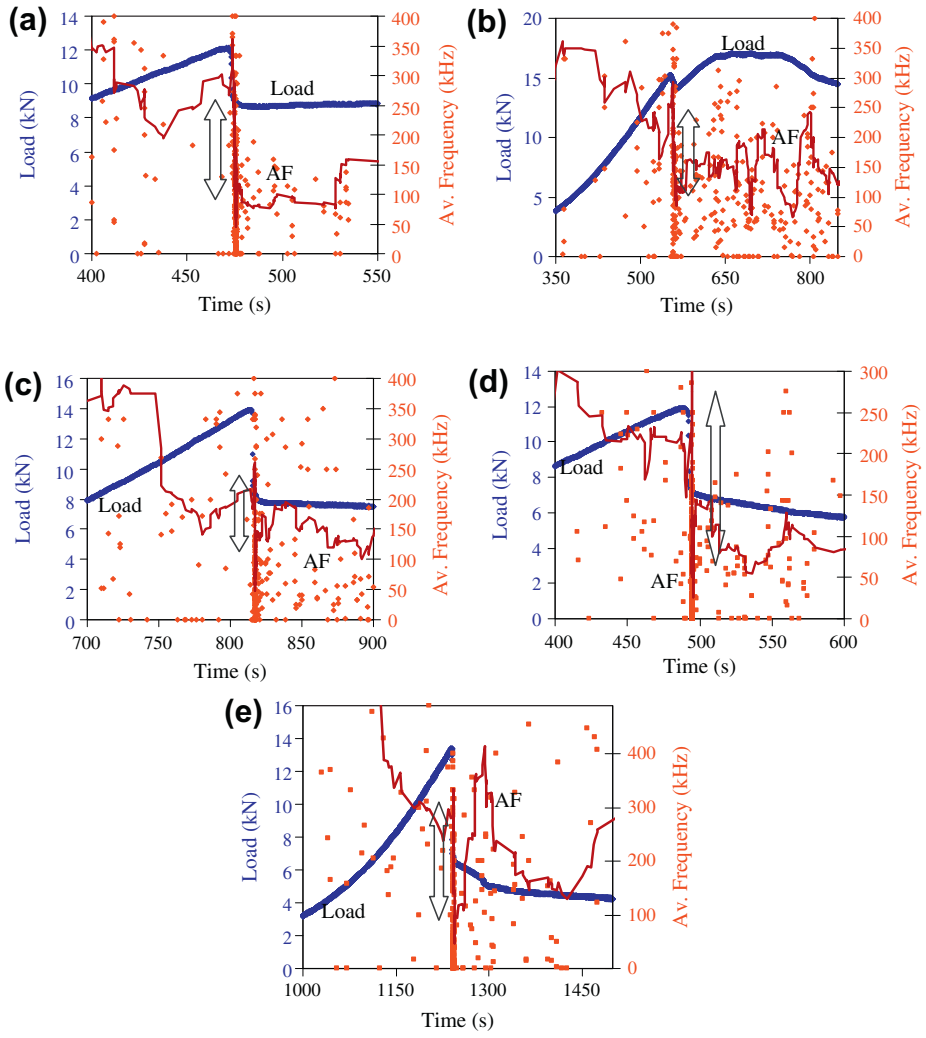

Fig. 5. Load and average frequency history for all specimens.

fracture moment is not an issue due to the load drop, as well as, the appearance of visible cracks, this is not always the case for a real structure where a similar crack will not produce visible deflection. Therefore, the sudden drop of the I*b*-value will indicate the upcoming failure with the minimum value itself being related to the severity of the structural condition of the material around the sensors. It is mentioned that the actually monitored volume cannot be accurately calculated. It is considered however, that incidences that occur between the sensors are adequately captured, something that is supported by the numbers of AE activity as well as the high population of events identified by linear location algorithm between the two sensors. To the authors' knowledge this is the first application of I*b*-value analysis in SFRC and it shows the global validity of this index. However, it should be kept in mind that the contribution of fibres is not strong before the first macro-cracking incidence; the I*b*-value drop therefore, should be attributed to matrix cracking similarly to plain concrete.

3.2. Average frequency

Apart from the I*b*-value, another parameter that has been studied in respect to the failure mode is the average frequency (AF) of the signals [14,15]. This feature is calculated from the number of threshold crossings of the waveform divided by its duration. It has been shown that cracks resembling mode I (tensile) produce signals with relatively high frequency, while the shear type of crack (mode II) results in lower frequency. In the present case, the logical sequence of events starts with the type I matrix cracking which is initiated at the bottom surface due to tensile loads. As the crack extends to the top, fibre friction and pull-out events (shear, mode II) start to occur. At the last stage when most of the specimen's cross section has been ruptured and the two parts of the specimen get more separated, the fibre pull-out events dominate the process.

For the materials of this study, AF exhibited a consistent strong drop of approximately 200 kHz at the moment of main failure. This can be seen in Fig. 5a–e. The dots correspond to the AF of each AE hit while the solid line is the moving average of the recent 30 hits in order to show the trend clearly. The AF shift to lower values at the moment of failure is connected to the failure mechanism as discussed above. It is reasonable that prior to the main fracture, the matrix is being ruptured until the cracking zone reaches towards the top surface. After the main network of cracks has been developed, the tensile cracking events give their place gradually to the shear mode due to fibre debonding and friction which occurs during fibre pull out. This behaviour resembles the shear type of failure which is connected to low average frequency. In this case, due to the broadband response of the sensors this shift is adequately recorded, compared to the use of resonant sensors [15]. The downshift of frequency at the stage of fibre friction has also

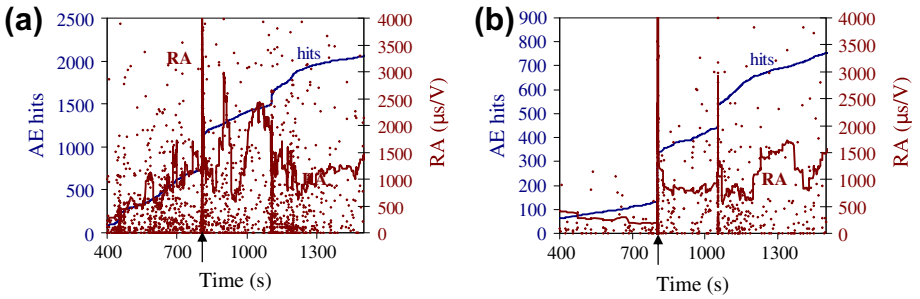

Fig. 6. (a and b) Cumulative AE hits and RA for two SFRC specimens. The moment of main fracture is marked by an arrow on the time axis.

Table 1
Average value of AE parameters for different fracturing stages.

Stage	AE hits	AF (kHz)	RA (μs/V)
Before main crack	144	307	1316
During crack formation	185	127	4419
After crack formation	272	203	1550

been reported in fibre pull out experiments [22]. It is mentioned that several fluctuations of the curve may be exhibited throughout the duration of the experiment (see Fig. 5). All should be attributed to the dynamic fracture behaviour; however, the moment of main fracture is the most indicative of the shift of the dominant failure mode from matrix cracking to fibre pull out and results in severe drops of the moving average of frequency in periods of less than one second. The frequency decreases from 250–320 kHz to the level of 50–100 kHz. It is mentioned that the actual frequency of the sources could be different than the one captured by the specific sensors. Although they are considered broadband still their frequency response should have an effect on the finally calculated parameters. However, since the behaviour of the specimens throughout the experimental series were recorded by the same set of sensors and acquisition parameters, any difference of average frequency is connected to the material condition itself, which except the changing of failure mode could even include the increasing attenuation due to accumulating damage.

3.3. RA value

As mentioned above, the shape of the AE waveforms is related to damage type and accumulation. The shape of the first part of the waveform is quantified by "RA" which is defined as the ratio of the waveform Rise Time to the Amplitude in μs/V. This value shifts to higher values as damage is being accumulated. Additionally, the transition of the fracture type from the initial tensile to the shear before failure also causes this kind of RA value shift [14,15]. Similar behaviour has been reported in laminated composites [5,23] concerning the shift from matrix cracking to delaminations. This can be simply explained by the wave modes excited by the different crack types; tensile cracks cause a transient volumetric change inside the material, converting the released energy mainly into a longitudinal (dilatational) wave. Therefore, the excited pulse contains longitudinal waves of large amplitude which are faster than any other type possibly excited and the resulting Rise Time is short. On the other hand in the case of a shear crack, although longitudinal waves may still be excited, most of the energy is transmitted as shear waves which are slower; thus the major part of the energy (or maximum amplitude) arrives later than the first longitudinal arrivals resulting in longer Rise Time. Fig. 6a and b shows two typical cases of RA moving average with time along

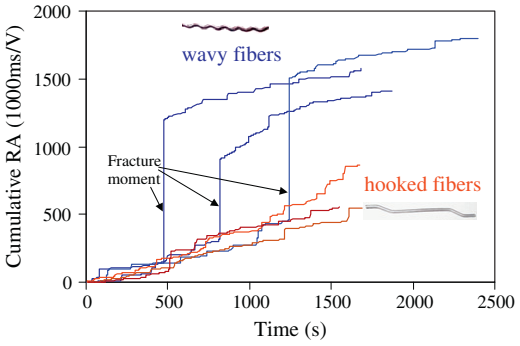

Fig. 7. Cumulative RA for different SFRC specimens.

with the cumulative AE hits. Before the main fracture event which is demonstrated by a sudden, almost vertical increase in AE hits, RA averages around 500 μs/V. At the moment of main fracture it exhibits strong local maxima and afterwards it exhibits some fluctuations on a generally increasing trend, usually reaching 2000 μs/V. This trend has been also observed on vinyl fibre concrete [21], and shows that different mechanisms inside the material produce different signature AE signals. Table 1 includes the average values of AE parameters for the three distinct failure stages (before main crack formation, during and after). It is stressed out that the 2nd stage lasts for about 1 s, while more than 100 hits are typically recorded in its duration. Additionally, the drop of AF (by 60%) and the rise of RA (by more than 200%) compared to the initial stage are evident for the 2nd (macro-cracking) stage. For the final stage the values are partially restored towards the initial values.

In this point, it is important to indicatively discuss the behaviour of specimens with different shape of fibres at the moment of main fracture. In the experimental series, another shape of fibres was used, namely fibres with hooked ends. Their length was 30 mm. These fibres did not exhibit strong RA maxima at the moment of main crack formation. Fig. 7 shows the cumulative RA value history for six different specimens with 1% of fibres; three with wavy fibres and three with hooked fibres. It is obvious that for all wavy fibre specimens there is a sharp increase of RA which occurs at the moment of main fracture, indicating strong shear actions. For the hooked fibres though, the curve is much smoother without sharp peaks at any moment, indicating that the fracture process and the corresponding crack propagation incidences are smoother with this kind of fibres. It is characteristic that concerning the whole duration of the experiment, the value of RA from the total number of hits averages at 4946 μs/V for the wavy fibre specimens, while it averages only at 1064 μs/V for specimens with hooked fibres. This discrepancy in the value of AE parameters between the different fibre shapes indicates different mechanical and fracturing behaviour as well.

4. Conclusions

In the present study AE indices are used to characterize the damage process of steel fibre reinforced concrete. The I*b*-value which depends on the amplitude distribution of the AE hits shows a consistent trend of decreasing earlier than 80% of the fracture load, acting as a warning. Furthermore, it obtains its minimum at the moment of fracture, behaviour which is very useful in the case of remote monitoring of large structures. Additionally, the average frequency of the AE hits as recorded by broadband sensors shows a severe shift to lower values by about 200 kHz when the dominant failure mechanism shifts from tensile micro-cracking, to macro-cracking with fibre pull out. Similarly RA shows strong peaks at the moments of fracture indicating shear action while it exhibits distinct behaviour for different types of fibres. Further study should be conducted in order to expand to different fibre volumes and shapes and also challenge the use of broadband sensors for AE monitoring of larger specimens.

Acknowledgements

The fibres were kindly supplied by ETAL S.A., Greece and CHIR-CU PROD-IMPEX COMPANY SRL, Romania.

References

[1] Stahli P, van Mier JGM. Manufacturing, fibre anisotropy and fracture of hybrid fibre concrete. Eng Fract Mech 2007;74:223–42.
[2] Kumar A, Gupta AP. Acoustic emission in fibre reinforced concrete. Exp Mech 1996;36(3):258–61.
[3] Bentahar M, Gouerjuma RE. Monitoring progressive damage in polymer based composite using nonlinear dynamics and acoustic emission. J Acoust Soc Am 2009;125:EL39–44.
[4] Farrelly FA, Petri A, Pitolli L, Pontuale G, Tagliani A, Novi Inverardi PL. Statistical properties of acoustic emission signals from metal cutting processes. J Acoust Soc Am 2004;116:981–6.
[5] Anastassopoulos AA, Philippidis TP. Clustering methodology for evaluation of acoustic emission from composites. J Acoust Emiss 1995;13(1/2):11–22.
[6] Yuyama S, Imanaka T, Ohtsu M. Quantitative evaluation of microfracture due to disbonding by waveform analysis of acoustic emission. J Acoust Soc Am 1988;83:976–83.
[7] Shiotani T, Bisschop J, Van Mier JGM. Temporal and spatial development of drying shrinkage cracking in cement-based materials. Eng Fract Mech 2003;70(12):1509–25.
[8] Luo X, Haya H, Inaba T, Shiotani T. Seismic diagnosis of railway substructures by using secondary acoustic emission. Soil Dyn Earthquake Eng 2006;26:1101–10.
[9] Colombo S, Main IG, Forde MC. Assessing damage of reinforced concrete beam using "b-value" analysis of acoustic emission signals. J Mater Civil Eng 2003;15(3):280–6.
[10] Ohtsu M, Uchida M, Okamoto T, Yuyama S. Damage assessment of reinforced concrete beams qualified by acoustic emission. ACI Struct J 2002;99(4):411–7.
[11] Schechinger B, Vogel T. Acoustic emission for monitoring a reinforced concrete beam subject to four-point-bending. Constr Build Mater 2007;21(13):483–90.
[12] Colombo S, Forde MC, Main IG, Shigeishi M. Predicting the ultimate bending capacity of concrete beams from the 'Relaxation Ratio' analysis of AE signals. Constr Build Mater 2005;19:746–54.
[13] Grosse CU, Reinhardt HW, Dahm T. Localization and classification of fracture types in concrete with quantitative acoustic emission measurement techniques. NDT&E Int 1997;30(4):223–30.
[14] Ohtsu M, Tomoda Y. Phenomenological model of corrosion process in reinforced concrete identified by acoustic emission. ACI Mater J 2008;105(2):194–9.
[15] Soulioti D, Barkoula NM, Paipetis A, Matikas TE, Shiotani T, Aggelis DG. Acoustic emission behaviour of steel fibre reinforced concrete under bending. Constr Build Mater 2009;23:3532–6.
[16] Soulioti DV, Barkoula NM, Paipetis A, Matikas TE. Effects of fibre geometry and volume fraction on the flexural behaviour of steel–fibre reinforced concrete. Strain, in press. doi: 10.1111/j.1475-1305.2009.00652.x.
[17] Ohtsu M. (Chairman). Recommendations of RILEM Technical Committee 212-ACD: acoustic emission and related NDE techniques for crack detection and damage evaluation in concrete: 3. Test method for classification of active cracks in concrete structures by acoustic emission. Mater Struct 2010;43(9):1187–9.
[18] Shiotani T, Ohtsu M, Ikeda K. Detection and evaluation of AE waves due to rock deformation. Constr Build Mater 2001;15(5–6):235–46.
[19] Kurz JH, Finck F, Grosse CU, Reinhardt HW. Stress drop and stress redistribution in concrete quantified over time by the b-value analysis. Struct Health Monit 2005;5:69–81.
[20] Shiotani T, Fujii K, Aoki T, Amou K. Evaluation of progressive failure using AE sources and improved B-value on slope model tests. Prog Acoust Emiss 1994;7:529–34.
[21] Aggelis DG, Shiotani T, Momoki S, Hirama A. Acoustic emission and ultrasound for damage characterization of concrete elements. ACI Mater J 2009;106(6):509–14.
[22] Reinhardt HW, Grosse CU, Weiler B. Material characterization of steel fibre reinforced concrete using neutron CT, ultrasound and quantitative acoustic emission techniques. NDT.net 2001;6(5). <http://www.ndt.net/article/v06n05/grosse/grosse.htm>.
[23] Aggelis DG, Barkoula NM, Matikas TE, Paipetis AS. Acoustic emission monitoring of degradation of cross ply laminates. J Acoust Soc Am. 2010;127(6):EL246–51.